Trabajo de Fin de Grado

Solution of quantum-mechanical problems with the R-matrix method

Pablo Manuel Pérez Peinado

UNIVERSIDAD Ð SEVILLA

Supervisors:

Dr. José A. Lay Valera and Dr. Antonio M. Moro Muñoz

Universidad de Sevilla

Facultad de Física

Departamento de Física Atómica, Molecular y Nuclear

Seville, June 2021

Acknowledgements

This work would not have seen the light of day without the help of many people that propelled me and stood by my side when things got complicated. Firstly I would like to thank my supervisors Dr. José A. Lay Valera and Dr. Antonio M. Moro Muñoz for encouraging me all along during the time it took me to write this report, their engagement regarding my understanding of the present subject and the guidance they offered me when obstacles were met were of a great scientific, professional and human value. I am very grateful for everything they taught me and for the effort they put into this project.

Of course the present survey would not exist without the aid of my mother, my father, my brother and all my close friends who, -even though unfamiliar with all the intricate details I could bring up when asked if I needed any help- were undoubtedly the greatest of supports any scientific mind still in formation could wish for. Thanks enormously to all of you. Muchas gracias.

Contents

Chapter 1

Introduction

The R-matrix method or R-matrix theory is a powerful tool that describes scattering states resulting from the interaction of systems of particles [1]. This theory was firstly presented by Wigner and Eisenbud [2–4], whose simplification of the original idea by Kapur and Peierls [5] is that the R-matrix is real.

Among motivations for treating this method one finds the fact that it is a concise and straightforward way to solve the Schrödinger equation of a large selection of Nuclear Physics and Atomic Physics problems, and that it represents an approach to study the continua of systems, contrasting with only dealing with a discrete set of bound states. Namely, two systems will be studied in this work: the narrow scattering resonances of the ^{12}C+p system [1] with total angular momentum and parity $J^{\pi} = 1/2^{+}$, and the ^{10}Be+n system [6] with $J^{\pi} = 5/2^{+}$. The ^{11}Be nuclide is a halo nucleus which is regarded as a compound ^{10}Be+n system in this work. A halo is produced when one or few nucleons in a nucleus are so barely bound that their wave functions can explore large distances from the rest of nucleons. The latter form a tight structure, usually called core, and the extensive wave function can be seen as a diluted halo of matter around that core. Thus, in addition, analysing the behaviour of a halo nucleus is another incentive to the fulfilment of this dissertation.

One should distinguish between two different kinds of R-matrix variants: the 'phenomenological' and 'calculable' one. The phenomenological R-matrix consists in a procedure to parametrize several types of cross sections, used mainly in Nuclear Physics. Instead, the calculable R-matrix is an analytical method which enables calculations of scattering properties in a great amount of physical problems. Although the R-matrix

method could equally treat bound states, here only cases with positive relative energies ($E > 0$) will be studied. Furthermore, this dissertation will only deal with two-body problems of inert particles.

The R-matrix principle may be explained as follows: The time-independent Schrödinger equation is a second-order partial differential equation which can be solved by means of different numerical methods, such as Numerov's or Runge-Kutta's. These methods present computational drawbacks when either fine resolution or large distances calculations are required. In contrast, the calculable R-matrix method is analytical, which means that it is not affected by these inconveniences.

For each separate case, the R-matrix theory uses a potential that describes specific properties of the system, and satisfies certain asymptotic conditions. It assumes potentials differing at most from the Coulomb potential by the inverse square of the relative distance between particles r. This additional term is the short-range potential. Explicitly:

$$V(r) = V_C(r) + V'(r) \; ; V'(r) \xrightarrow[r \to \infty]{} O(r^{-2}) \; , \tag{1.1}$$

where V_C, V' are the Coulomb and short-range potentials respectively. One chooses thus a boundary a of the relative distance, called the channel radius, that separates the configuration space into an internal and an external region, as in figure 1.1. In the external region the short-range potential is negligible, and the solution to the Schrödinger equation there may be taken as its asymptotic form. Unbound asymptotic solutions include a quantity called phase shift, which characterises them. Besides, the system is considered
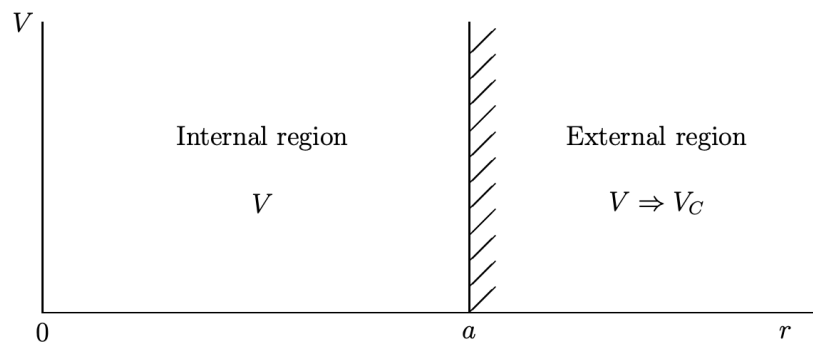

Figure 1.1: The R-matrix method: Visualization of the boundary, from [7].

as confined in the internal region, so that the internal wave function can be expanded over a finite square-integrable basis, of dimension N. In this zone, the full interaction is taken into account. The elegant simplification the R-matrix theory provides is of great aid.

3

Basically one is able to calculate scattering properties reducing the number of relevant parameters to the channel radius a and the number N of eigenstates of the finite basis.

The main goal of this work is to generate a code which is able to apply the R-matrix method to a short-range potential that correctly simulates specific states of a system. Succeeding at this task will enable the calculation of scattering properties, such as resonance energies. To this end, the computer software MATLAB® was used, hence developments of R-matrix codes for this computational tool have been performed.

The calculable R-matrix version was first presented by Haglund and Robson in 1956, in an application to two-channel, square-well-potentials systems [8]. Expansion of the internal wave over a finite basis was proposed by Buttle [9]. Although it was originally conceived for application to Nuclear Physics, one finds important applications of the calculable R-matrix theory to Atomic Physics problems [10–12] where complex aspects as the non-locality and spin interaction are carefully treated with the help of propagation methods. Likewise, extensions of the R-matrix theory to the Dirac equation have been carried out [13, 14]. Finally, it is worth mentioning that usually R-matrix methods are used in multichannel processes, in which case it greatly simplifies calculations. Its main advantages are more easily shown in one-channel problems though, therefore its application in this work.

Chapter 2

Theoretical framework

In this chapter, the fundamental concepts of quantum scattering are reviewed, and subsequently the calculable R-matrix theory is shown more precisely for scattering states ($E > 0$). In particular, the importance of the Bloch operator is highlighted and several definitions such as that of the phase shift or the scattering matrix are mathematically expressed. Nuclear resonances are also briefly treated, highlighting several definitions of resonance energies. Choices of basis functions are also presented featuring its main properties regarding numerical calculations for applications.

2.1 Scattering theory

Considering the existence of a large and rich literature on the present subject [15–17], this section intends to display a succinct presentation of collision theory of two-body systems based mainly on [1] and the mathematical language followed in [18, 19].

Let two particles of masses m_1, m_2, charges eZ_1, eZ_2 ($e > 0$), and corresponding reduced mass $\mu = \frac{m_1 m_2}{m_1 + m_2}$ collide in the center-of-mass frame at positive energy E. The wavenumber is defined as:

$$k = \frac{\sqrt{2\mu E}}{\hbar} \ ,$$

(2.1)

a Bohr radius can be defined:

$$a_B = \frac{\hbar^2}{\mu |Z_1 Z_2| e^2} \ ,$$

(2.2)

and also the so-called Sommerfeld parameter:

$$\eta = \frac{Z_1 Z_1 e^2}{\hbar v} = \frac{\text{sign}(Z_1 Z_2)}{a_B k} \ ,$$

(2.3)

where $v = \frac{\hbar k}{\mu}$ is the relative speed between particles and η can be understood as a measure of the strength of the Coulomb interaction. Its value determines if the Coulomb force is repulsive ($\eta > 0$), attractive ($\eta < 0$) or none ($\eta = 0$). The Schrödinger equation describing the system is:

$$i\hbar \frac{\partial \Psi(\vec{r}, t)}{\partial t} = \left[-\frac{\hbar^2}{2\mu} \nabla^2 + V(r) \right] \Psi(\vec{r}, t) \ . \tag{2.4}$$

Potentials are supposed to be time-independent and spherically symmetrical, so that variable separation can be performed and the wave function can be written as:

$$\Psi(\vec{r}, t) = e^{-\frac{i}{\hbar} Et} \psi(\vec{r}) = e^{-\frac{i}{\hbar} Et} r^{-1} u(r) Y(\theta, \varphi) \tag{2.5}$$

where $Y(\theta, \varphi) = Y_{l,m}(\theta, \varphi) = Y_{l,m}(\Omega)$ are the spherical harmonics defined for angular momentum $l = 0, 1, 2, \ldots$ and its projection on the z axis $m = 0, \pm 1, \pm 2, \ldots, \pm l$. The partial wave function $u(r) = u_l(r)$ obeys the radial equation:

$$\left[-\frac{\hbar^2}{2\mu} \frac{\mathrm{d}^2}{\mathrm{d}r^2} + \frac{l(l+1)\hbar^2}{2\mu r^2} + V(r) \right] u_l(r) = \left[T_l + V(r) \right] u_l(r) = E u_l(r) \ , \tag{2.6}$$

defining the angular-momentum-dependent radial kinetic energy:

$$T_l = -\frac{\hbar^2}{2\mu} \left(\frac{\mathrm{d}^2}{\mathrm{d}r^2} - \frac{l(l+1)}{r^2} \right) \ . \tag{2.7}$$

Equation (2.6) multiplied by $-\frac{2\mu}{\hbar^2}$ at both sides and then brought in to the LHS yields the more concise form:

$$\left[\frac{\mathrm{d}^2}{\mathrm{d}r^2} - \frac{l(l+1)}{r^2} - \frac{2\mu V(r)}{r} + k^2 \right] u_l(r) = 0 \ , \tag{2.8}$$

with the condition $u_l(0) = 0$.

2.1.1 Unbound states

When only the Coulomb potential is considered, $V = V_C(r)$, equation (2.8) reads:

$$\left[\frac{\mathrm{d}^2}{\mathrm{d}r^2} - \frac{l(l+1)}{r^2} - \frac{2k\eta}{r} + k^2 \right] u_l(r) = 0 \ , \tag{2.9}$$

and positive energy solutions to this equation are combinations of regular $F_l(\eta, kr)$ and irregular $G_l(\eta, kr)$ Coulomb functions [18] (see figure 2.1), whose behaviour at large values of $\rho = kr$, $\rho = kr \to \infty$ is:

$$\begin{cases} F_l(\eta, \rho) \xrightarrow[\rho \to \infty]{} \sin\left(\rho - \frac{\pi}{2} - \eta \ln 2\rho + \sigma_l(\eta)\right) & \text{(2.10a)} \\ G_l(\eta, \rho) \xrightarrow[\rho \to \infty]{} \cos\left(\rho - \frac{\pi}{2} - \eta \ln 2\rho + \sigma_l(\eta)\right) , & \text{(2.10b)} \end{cases}$$

where

$$\sigma_l(\eta) = \arg[\Gamma(l + 1 + i\eta)] \tag{2.11}$$

is the Coulomb phase shift, which includes the Euler gamma function Γ. It is customary also to introduce the conjugate functions:

$$\begin{cases} H_l^+(\eta, \rho) = O_l(\eta, \rho) = G_l(\eta, \rho) + iF_l(\eta, \rho) & \text{(2.12a)} \\ H_l^-(\eta, \rho) = I_l(\eta, \rho) = G_l(\eta, \rho) - iF_l(\eta, \rho) . & \text{(2.12b)} \end{cases}$$
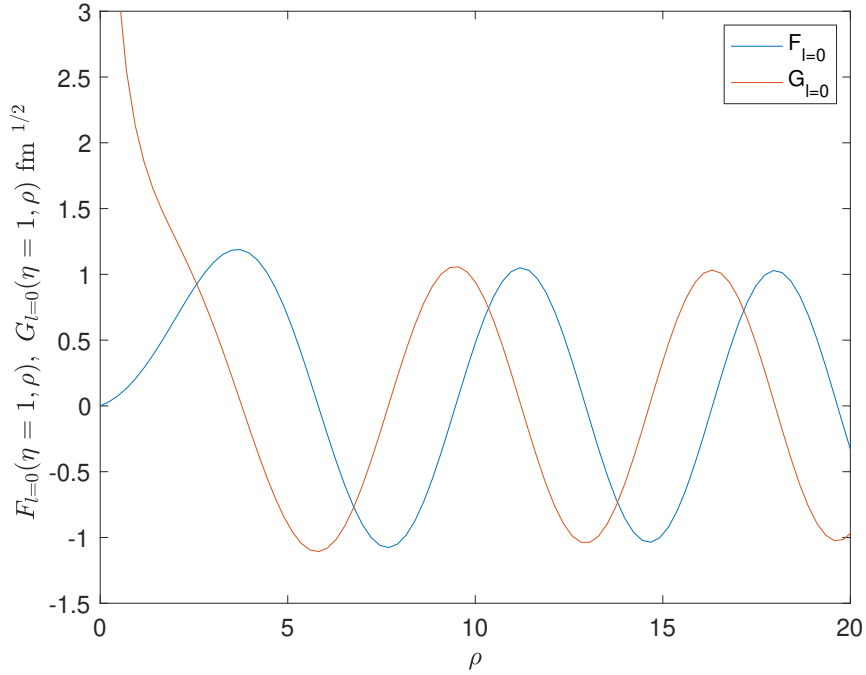

Figure 2.1: Unbound solutions to equation 2.9: F_l and G_l for $\eta = 1$, $l = 0$.

If a short-range potential $V'(r)$ term is added to the Coulomb potential:

$$V(r) = V_C(r) + V'(r) \; ; \; V'(r) \xrightarrow[r \to \infty]{} O(r^{-2}) , \tag{2.13}$$

the radial Schrödinger equation becomes:

$$\left[\frac{d^2}{dr^2} - \frac{l(l + 1)}{r^2} - \frac{2k\eta}{r} - \frac{2\mu V'(r)}{r} + k^2\right] u_l(r) = 0 , \tag{2.14}$$

and at positive energies solutions behave asymptotically as:

$$u_l(r) \xrightarrow[r \to \infty]{} \cos(\delta_l) F_l(\eta, kr) + \sin(\delta_l) G_l(\eta, kr) , \tag{2.15}$$

where the important physical quantity δ_l, called the phase shift, has been introduced by the addition of the short-range potential (see chapter 10 of [16], for example). The phase shift has the feature that it is positive or negative depending on whether the total potential is attractive or repulsive. Studying phase shifts, resonances can be found and characterised.

The scattering 'matrix' (it becomes a square matrix in multichannel processes) is defined as:

$$U_l = e^{2i\delta_l} \ , \tag{2.16}$$

and the asymptotic solution can be written more conveniently:

$$u_l(r) \xrightarrow[r\to\infty]{} C_l\big[I_l(\eta, kr) - U_l O_l(\eta, kr)\big] \ , \tag{2.17}$$

where C_l should be defined according to the chosen normalization. A convenient choice is $C_l = ie^{-i\delta_l}/2$ so that form (2.15) is recovered. Out of knowledge of this partial wave function, cross sections can be constructed [16].

2.2 Calculable R-matrix theory

As previously mentioned, two versions of the R-matrix theory exist differing on its method of application. However, even the phenomenological variant of the R-matrix theory needs the analytical expression of the theoretical one in order to be useful, therefore its derivation is of great importance. For this purpose one-channel processes will be assumed. In these collisions two particles interact through a central potential $V(r)$, which can be taken as the Coulomb potential for large r.

Equation (2.6) can be expressed as:

$$H_l u_l(r) = E u_l(r) \ , \tag{2.18}$$

where $H_l = T_l + V(r)$, and T_l is given in equation (2.7). The R-matrix method assumes that $u_l(r)$ is spanned for $r < a$ by an N-dimensional finite basis, so that the internal radial wave function is:

$$u_l(r) = u_l^{int}(r) = \sum_{j=1}^{N} c_j \varphi_j(r) \ ; \ r < a \ , \tag{2.19}$$

where the basis elements $\{\varphi_j(r)\}_{j=1}^{N}$ are all zero at the origin. In the present discussion they are not required to satisfy any particular condition (see pag. 12 of [1] for a discussion

about boundary conditions on basis functions). Neither do they need be orthogonal, even though they can be chosen that way in some cases.

The external radial wave function is approximated by its asymptotic form (2.17) (Sommerfeld parameter implied):

$$u_l(r) = u_l^{ext}(r) = C_l\big[I_l(kr) - U_l O_l(kr)\big] \ ; \ r > a \ . \tag{2.20}$$

Both forms of the radial wave function u_l are normalized carefully choosing C_l and considering that the basis $\{\varphi_j(r)\}_{j=1}^N$ is square-integrable. As usual, requirements that the wave function and its first derivative be continuous at $r = a$ hold:

$$u_l(a) = u_l^{int}(a) = u_l^{ext}(a) \ , \tag{2.21}$$

$$u_l'(a) = \left.\frac{\mathrm{d}u_l(r)}{\mathrm{d}r}\right|_{r=a} = \left.\frac{\mathrm{d}u_l^{int}(r)}{\mathrm{d}r}\right|_{r=a} = \left.\frac{\mathrm{d}u_l^{ext}(r)}{\mathrm{d}r}\right|_{r=a} . \tag{2.22}$$

The R-matrix $R_l(E)$ at energy E is defined by means of:

$$u_l(a) = R_l(E)\big[au_l'(a) - Bu_l(a)\big] \ , \tag{2.23}$$

where B is the boundary parameter appearing in the Bloch operator (see subsection 2.2.1) whose choice is to be discussed later on. Let it be remarked that R_l is dimensionless, differing from definitions by other papers.

The principle of the theory consists on the fact that the R-matrix can be calculated from properties of the hamiltonian for $r < a$, and that knowing R_l enables the calculation of the scattering matrix U_l.

Taking into consideration that working with radial wave functions transforms scalar products of internal functions into:

$$\langle u_1 | u_2 \rangle = \int_0^a u_1^*(r) u_2(r) \mathrm{d}r \ , \tag{2.24}$$

one notices the hamiltonian is not hermitian over $(0, a)$, which turns out to be inconvenient when solving the Schrödinger equation.

Indeed one has $H_l = \mathcal{D} + \mathcal{U}_l(r)$, where these the operators are:

$$\mathcal{D} = T_0 = -\frac{\hbar^2}{2\mu}\frac{\mathrm{d}^2}{\mathrm{d}r^2} \ , \tag{2.25}$$

$$\mathcal{U}_l(r) = \frac{\hbar^2}{2\mu}\frac{l(l+1)}{r^2} + V(r) \ . \tag{2.26}$$

Evidenlty operator (2.26) is hermitian since its a sum of real-valued functions of r. Hermiticity or non-hermiticity of operator $\mathcal{D}$ is still to be determined.

Recalling the definition of the adjoint of an operator:

$$\langle u_1|\mathcal{D}|u_2\rangle^* = \langle u_2|\mathcal{D}^\dagger|u_1\rangle = \int \mathrm{d}r \ u_2^*(\mathcal{D}^\dagger u_1) = \left[\int \mathrm{d}r \ u_1^*(\mathcal{D}u_2)\right]^*$$

$$= \int \mathrm{d}r \ u_1(\mathcal{D}u_2)^* = \int \mathrm{d}r \ (\mathcal{D}u_2)^* u_1 \ , \tag{2.27}$$

where the integration domain is $(0,a)$. Assuming $\mathcal{D} = \mathcal{D}^\dagger$ yields:

$$\langle u_2|\mathcal{D}^\dagger|u_1\rangle = \langle u_2|\mathcal{D}|u_1\rangle = \int \mathrm{d}r \ u_2^*(\mathcal{D}u_1) = \int \mathrm{d}r \ (\mathcal{D}u_2)^* u_1$$

$$= -\frac{\hbar^2}{2\mu}\int \mathrm{d}r \ u_2^*\frac{\mathrm{d}^2 u_1}{\mathrm{d}r^2} = -\frac{\hbar^2}{2\mu}\int \mathrm{d}r \ u_1\frac{\mathrm{d}^2 u_2^*}{\mathrm{d}r^2}. \tag{2.28}$$

Thus one would demonstrate that $\mathcal{D} = \mathcal{D}^\dagger$ if:

$$\int \mathrm{d}r \ \left(u_2^*\frac{\mathrm{d}^2 u_1}{\mathrm{d}r^2} - u_1\frac{\mathrm{d}^2 u_2^*}{\mathrm{d}r^2}\right) = 0 \ . \tag{2.29}$$

However it is found that:

$$\int \mathrm{d}r \ \left(u_2^*\frac{\mathrm{d}^2 u_1}{\mathrm{d}r^2} - u_1\frac{\mathrm{d}^2 u_2^*}{\mathrm{d}r^2}\right)$$

$$= \int \mathrm{d}r \ \left\{\frac{\mathrm{d}}{\mathrm{d}r}\left[\frac{\mathrm{d}u_1 u_2^*}{\mathrm{d}r}\right]\right\} - 2\int \mathrm{d}r \ \frac{\mathrm{d}^2 u_2^*}{\mathrm{d}r^2}u_1 - 2\int \mathrm{d}r \ \frac{\mathrm{d}u_2^*}{\mathrm{d}r}\frac{\mathrm{d}u_1}{\mathrm{d}r}$$

$$= \left[\frac{\mathrm{d}(u_1 u_2^*)}{\mathrm{d}r}\right]_0^a - 2\int \mathrm{d}r \ \frac{\mathrm{d}}{\mathrm{d}r}\left(\frac{\mathrm{d}u_2^*}{\mathrm{d}r}u_1\right) \ . \tag{2.30}$$

Bearing in mind that all radial wave functions u_1, u_2 are required to be null at the origin and that their derivatives must be finite at all points in the domain, this is equal to the Wronskian $\mathcal{W}$ of the two functions at $r = a$:

$$\int \mathrm{d}r \ \left(u_2'^*\frac{\mathrm{d}^2 u_2}{\mathrm{d}r^2} - u_1\frac{\mathrm{d}^2 u_1^*}{\mathrm{d}r^2}\right) = \mathcal{W}\{u_2^*, u_1\}(a) = u_2^*(a)u_1'(a) - u_2'^*(a)u_1(a) \ , \tag{2.31}$$

different from zero in general. So it follows that $\mathcal{D} \neq \mathcal{D}^\dagger$, and H_l is not hermitian over $(0,a)$.

2.2.1 The Bloch Operator $\mathcal{L}_B(r)$

The surface operator introduced by Bloch [1, 20] is defined as:

$$\mathcal{L}_B(r) = \frac{\hbar^2}{2\mu}\delta(r-a)\left(\frac{\mathrm{d}}{\mathrm{d}r} - \frac{B}{r}\right) \ , \tag{2.32}$$

where the boundary parameter B appearing in equation (2.23) is real so that the operator $H_l + \mathcal{L}_B(r)$ is hermitian over $(0, a)$. Indeed one may carry out the calculations in equation (2.28) replacing $\mathcal{D}$ with $\mathcal{D} + \mathcal{L}_B(r)$:

$$
\begin{aligned}
\langle u_2 | (\mathcal{D} + \mathcal{L}_B(r))^\dagger | u_1 \rangle &= \langle u_2 | \mathcal{D} + \mathcal{L}_B(r) | u_1 \rangle \\
&= \int \mathrm{d}r \; u_2^* [(\mathcal{D} + \mathcal{L}_B(r)) u_1] = \int \mathrm{d}r \; [(\mathcal{D} + \mathcal{L}_B(r)) u_2]^* u_1 \;, \quad (2.33)
\end{aligned}
$$

which amounts to ensuring that the following relation holds:

$$
\int \mathrm{d}r \; \left\{ u_2^* \Big[\frac{\mathrm{d}^2}{\mathrm{d}r^2} - \delta(r-a) \Big(\frac{\mathrm{d}}{\mathrm{d}r} - \frac{B}{r} \Big) \Big] u_1 - u_1 \Big[\frac{\mathrm{d}^2}{\mathrm{d}r^2} - \delta(r-a) \Big(\frac{\mathrm{d}}{\mathrm{d}r} - \frac{B}{r} \Big) \Big] u_2^* \right\} = 0 \;.
$$
$$(2.34)$$

Calculating explicitly one finds this is the case:

$$
\begin{aligned}
\int \mathrm{d}r \; &\left\{ u_2^* \Big[\frac{\mathrm{d}^2}{\mathrm{d}r^2} - \delta(r-a) \Big(\frac{\mathrm{d}}{\mathrm{d}r} - \frac{B}{r} \Big) \Big] u_1 - u_1 \Big[\frac{\mathrm{d}^2}{\mathrm{d}r^2} - \delta(r-a) \Big(\frac{\mathrm{d}}{\mathrm{d}r} - \frac{B}{r} \Big) \Big] u_2^* \right\} \\
&= \mathcal{W}\{u_2^*, u_1\}(a) \\
&+ \int \mathrm{d}r \; u_1 \delta(r-a) \Big(\frac{\mathrm{d}u_2^*}{\mathrm{d}r} - \frac{B}{r} u_2^* \Big) - \int \mathrm{d}r \; u_2^* \delta(r-a) \Big(\frac{\mathrm{d}u_1}{\mathrm{d}r} - \frac{B}{r} u_1 \Big) \\
&= \mathcal{W}\{u_2^*, u_1\}(a) + u_1(a) \Big(u_2'^*(a) - \frac{B}{a} u_2^*(a) \Big) - u_2^*(a) \Big(u_1'(a) - \frac{B}{a} u_1(a) \Big) \\
&= \mathcal{W}\{u_2^*, u_1\}(a) + \mathcal{W}\{u_1, u_2^*\}(a) = 0 \;, \quad\quad (2.35)
\end{aligned}
$$

so the operator $H_l + \mathcal{L}_B(r)$ is hermitian over $(0, a)$.

Furthermore, this operator makes it possible for the Schrödinger equation (2.18) to be expressed differently in the internal region:

$$
\big(H_l + \mathcal{L}_B(r) - E \big) u_l^{int}(r) = \mathcal{L}_B(r) u_l^{ext}(r) \;; r < a \;, \quad\quad (2.36)
$$

which is named the Bloch-Schrödinger equation.

With the continuity condition:

$$
u_l^{int}(a) = u_l^{ext}(a) \;, \quad\quad (2.37)
$$

the problem is totally equivalent to equation (2.18) in the interval $(0, a)$ provided with the condition of continuous derivative:

$$
u_l'^{int}(a) = u_l'^{ext}(a) \;. \quad\quad (2.38)
$$

In fact, integrating equation (2.36) and using relation (2.37) ensures derivative continuity straightforwardly. Hence, not only does the Bloch operator enable hermiticity over $(0, a)$, but it guarantees the continuity of the wave function's derivatives as well.

The inhomogeneous Bloch-Schrödinger equation (2.36) can be formally solved by means of the Green function $G_l(r, r')$ defined by:

$$\left(H_l + \mathcal{L}_B(r) - E\right)G_l(r, r') = \delta(r - r') \ ; \ G_l(0, r) = 0 \ . \tag{2.39}$$

Indeed, if one applies operator $\left(H_l + \mathcal{L}_B(r) - E\right)$ to the r-dependent function $\int_0^a \mathrm{d}r' \ G_l(r, r')\mathcal{L}_B(r')u_l^{ext}(r')$, one obtains:

$$\left(H_l + \mathcal{L}_B(r) - E\right)\int_0^a \mathrm{d}r' \ G_l(r, r')\mathcal{L}_B(r')u_l^{ext}(r')$$

$$= \int_0^a \mathrm{d}r'\left(H_l + \mathcal{L}_B(r) - E\right)G_l(r, r')\mathcal{L}_B(r')u_l^{ext}(r') = \int_0^a \mathrm{d}r'\delta(r - r')\mathcal{L}_B(r')u_l^{ext}(r')$$

$$= \mathcal{L}_B(r)u_l^{ext}(r) \ , \tag{2.40}$$

since H_l is only r-dependent. Thus it is possible to write the internal solution as:

$$u_l^{int}(r) = \int_0^a \mathrm{d}r' \ G_l(r, r')\mathcal{L}_B(r')u_l^{ext}(r') \ , \tag{2.41}$$

that is,

$$u_l^{int}(r) = \int_0^a \mathrm{d}r' \ G_l(r, r')\frac{\hbar^2}{2\mu}\delta(r - a)\left(\frac{\mathrm{d}}{\mathrm{d}r'} - \frac{B}{r'}\right)u_l^{ext}(r')$$

$$= G_l(r, a)\frac{\hbar^2}{2\mu a}\left(au_l'^{ext}(a) - Bu_l^{ext}(a)\right) \ . \tag{2.42}$$

Therefore with the aid of equation (2.23), the R-matrix is simply:

$$R_l(E) = \frac{\hbar^2}{2\mu a}G_l(a, a) \ . \tag{2.43}$$

Additionally, practical expressions for $R_l(E)$ are obtained by plugging expansion (2.19) into equation (2.36) and projecting its result upon a certain basis element $\varphi_i(r)$, which yields:

$$\sum_{j=1}^N \mathbf{C}_{ij}(E, B)c_j = \frac{\hbar^2}{2\mu a}\varphi_i(a)\left(au_l'^{ext}(a) - Bu_l^{ext}(a)\right) \ , \tag{2.44}$$

where the symmetric matrix $\mathbf{C}$ is defined as:

$$\mathbf{C}_{ij}(E, B) = \langle\varphi_i|T_l + \mathcal{L}_B(r) + V - E|\varphi_j\rangle \ . \tag{2.45}$$

Defining a vector $\vec{\xi}$ whose elements are:

$$\xi_i = \frac{\hbar^2}{2\mu a}\varphi_i(a)\left(au_l'^{ext}(a) - Bu_l^{ext}(a)\right) \ ; \ i = 1, \ldots, N \ , \tag{2.46}$$

it is possible to formulate equation (2.44) in matrix form:

$$\mathbf{C}\vec{c} = \vec{\xi} \Rightarrow \vec{c} = \mathbf{C}^{-1}\vec{\xi} \, , \tag{2.47}$$

which means that the c_j coefficients are:

$$c_j = \sum_{k=1}^{N}(\mathbf{C}^{-1})_{jk}\xi_k = \sum_{k=1}^{N}(\mathbf{C}^{-1})_{jk}\frac{\hbar^2}{2\mu a}\frac{u_l(a)}{R_l(E)}\varphi_k(a) \, . \tag{2.48}$$

Changing dummy indexes, the internal wave function can thus be expressed in these terms:

$$u_l^{int}(r) = \sum_{i,j=1}^{N}(\mathbf{C}^{-1})_{ij}\frac{\hbar^2}{2\mu a}\varphi_i(a)\frac{u_l(a)}{R_l(E)}\varphi_j(r) \, , \tag{2.49}$$

which for $r = a$ results in:

$$u_l^{int}(a) = \sum_{i,j=1}^{N}(\mathbf{C}^{-1})_{ij}\frac{\hbar^2}{2\mu a}\varphi_i(a)\frac{u_l(a)}{R_l(E)}\varphi_j(a) = R_l(E)\Big(au_l'(a) - Bu_l(a)\Big) \, , \tag{2.50}$$

and therefore the calculable R-matrix is:

$$R_l(E, B) = \frac{\hbar^2}{2\mu a}\sum_{i,j=1}^{N}\varphi_i(a)(\mathbf{C}^{-1})_{ij}\varphi_j(a) = \frac{\hbar^2}{2\mu a}\vec{\varphi}^T(a)\mathbf{C}^{-1}(E, B)\vec{\varphi}(a) \, , \tag{2.51}$$

where $\vec{\varphi}(a)$ is the column vector composed of all N basis elements $\varphi_i(r)$ at $r = a$. Finally the internal wave function is given by:

$$u_l^{int}(r) = \frac{\hbar^2}{2\mu a}\frac{u_l(a)}{R_l(E, B)}\sum_{i,j=1}^{N}\varphi_i(a)(\mathbf{C}^{-1})_{ij}\varphi_j(r) \, . \tag{2.52}$$

Orthonormal basis

Let the basis set $\{\varphi_j(r)\}_{j=1}^{N}$ be orthogonal and normalized to unity so that

$$\langle\varphi_i|\varphi_j\rangle = \delta_{ij} \; ; \; i, j = 1, \ldots, N \tag{2.53}$$

is satisfied. One focuses now on calculating the eigenvalues and eigenvectors of matrix $\mathbf{C}(0, B)$:

$$\mathbf{C}(0, B)\vec{v}_{nl} = E_{nl}\vec{v}_{nl} \, , \tag{2.54}$$

for angular momentum l. Eigenvectors are assumed to be normalized in the sense that:

$$\vec{v}_{nl}^T\vec{v}_{nl} = \delta_{nn'} \; ; \; n, n' = 1, \ldots, N \, . \tag{2.55}$$

Thus one finds:

$$\mathbf{C}(E,B)\vec{v}_{nl} = (E_{nl} - E)\vec{v}_{nl} \Rightarrow \vec{v}_{nl} = \frac{1}{E_{nl} - E}\mathbf{C}(E,B)\vec{v}_{nl}$$

$$\Rightarrow \mathbf{C}^{-1}(E,B)\vec{v}_{nl} = \frac{1}{E_{nl} - E}\vec{v}_{nl} \Rightarrow \mathbf{C}^{-1}(E,B)\Big(\sum_{n=1}^{N} \vec{v}_{nl}\vec{v}_{nl}^{T} \Big) = \sum_{n=1}^{N} \frac{\vec{v}_{nl}\vec{v}_{nl}^{T}}{E_{nl} - E} \ . \tag{2.56}$$

Now, it is straightforward that $\sum_{n=1}^{N} \vec{v}_{nl}\vec{v}_{nl}^{T} = \mathbb{1}$ since there are N N-dimensional eigenvectors $\vec{v}_{nl}$ and they are orthonormal with respect to each other, so finally the following spectral decomposition is verified:

$$\mathbf{C}^{-1}(E,B) = \sum_{n=1}^{N} \frac{\vec{v}_{nl}\vec{v}_{nl}^{T}}{E_{nl} - E} \ . \tag{2.57}$$

Keeping this result in mind, the R-matrix is obtained following equation (2.51):

$$R_l(E,B) = \frac{\hbar^2}{2\mu a}\vec{\varphi}^{T}(a)\Big(\sum_{n=1}^{N} \frac{\vec{v}_{nl}\vec{v}_{nl}^{T}}{E_{nl} - E} \Big)\vec{\varphi}(a)$$

$$= \frac{\hbar^2}{2\mu a}\Big(\sum_{n=1}^{N} \frac{\vec{\varphi}^{T}(a)\vec{v}_{nl}\vec{v}_{nl}^{T}\vec{\varphi}(a)}{E_{nl} - E} \Big) = \sum_{n=1}^{N} \frac{\gamma_{nl}^{2}}{E_{nl} - E} \ , \tag{2.58}$$

where

$$\gamma_{nl} = \sqrt{\frac{\hbar^2}{2\mu a}}\chi_{nl}(a) \ , \tag{2.59}$$

and with

$$\chi_{nl}(r) = \sum_{i=1}^{N} v_{nl,i}\varphi_i(r) \ , \tag{2.60}$$

$v_{nl,i}$ being the i-th component of $\vec{v}_{nl}$. The variables γ_{nl} are called the reduced width amplitudes whereas their squares γ_{nl}^{2} are named the reduced widths.

The quantities γ_{nl} have the following physical interpretation:

Up to a multiplicative constant $(\frac{\hbar^2}{2\mu a})^{1/2}$, they are the eigenvectors of operator $H_l + \mathcal{L}_B(r)$, expanded over the basis $\{\varphi_j(r)\}_{j=1}^{N}$ and evaluated at $r = a$. Since N is finite, the lowest-energy χ_{nl} eigenfunctions are approximated solutions of the problem confined over $r \in (0,a)$.

Last line of equations (2.58) is well-known in R-matrix theory, although its traditional expression makes N tend to infinity so that one obtains the exact eigenvalues and eigenfunctions of operator $H_l + \mathcal{L}_B(r)$:

$$R_l(E,B) = \sum_{n=1}^{\infty} \frac{\gamma_{nl}^{2}}{E_{nl} - E} \ . \tag{2.61}$$

Evidently, in practical terms, increasing N up to very large values entails very long computational times.

When V and B are complex, the extension of the R-matrix to the complex domain is direct [21].

2.2.2 The scattering matrix

With knowledge of the R-matrix, the scattering matrix $U_l(E)$ can be calculated considering (2.21) and plugging the external function (2.20) into relation (2.23), which yields:

$$
\begin{aligned}
R_l(E)\Big(au_l'^{ext}(a) - Bu_l^{ext}(a)\Big) &= u_l^{ext}(a) \\
&= R_l(E)\Big[kaC_l\Big(I_l'(ka) - U_lO_l'(ka)\Big) - BC_l\Big(I_l(ka) - U_lO_l(ka)\Big)\Big] \\
&= C_l\Big(I_l(ka) - U_lO_l(ka)\Big) .
\end{aligned}
\tag{2.62}
$$

After some operations one can find U_l from relation (2.62) and get:

$$
U_l(E) = e^{2i\phi_l}\frac{1 - (L_l^* - B)R_l(E)}{1 - (L_l - B)R_l(E)} ,
\tag{2.63}
$$

where $L_l = ka\left.\frac{\mathrm{d}\ln O_l(\rho)}{\mathrm{d}\rho}\right|_{\rho=ka}$ and

$$
\phi_l(E) = \arg\big[I_l(ka)\big] = \arctan\left[\frac{F_l(ka)}{G_l(ka)}\right]
\tag{2.64}
$$

is the hard-sphere phase shift. Furthermore, using the convenient property of the R-matrix (equation 3.27 in [1])

$$
\frac{1}{R_l(E,B)} = \frac{1}{R_l(E,B=0)} - B ,
\tag{2.65}
$$

it is shown right away that relation (2.63) does not depend on the value of the boundary parameter B, so that eventually taking $B = 0$ leads to the same scattering matrix. As it is the case for the scattering matrix and the external wave function, independence from B also applies to internal wave function (2.49) (equations (3.16), (3.27) and appendix B in [1]).

In order to get a deeper physical insight of results in applications, several definitions must be introduced. Accordingly, L_l is separated into its real and imaginary parts:

$$
L_l = S_l + iP_l ,
\tag{2.66}
$$

which are called the shift factor and penetration factor respectively. From previous definitions the penetration factor can be written as follows:

$$P_l(E) = \frac{ka}{|O_l(ka)|^2} = \frac{ka}{F_l^2(ka) + G_l^2(ka)} \ , \tag{2.67}$$

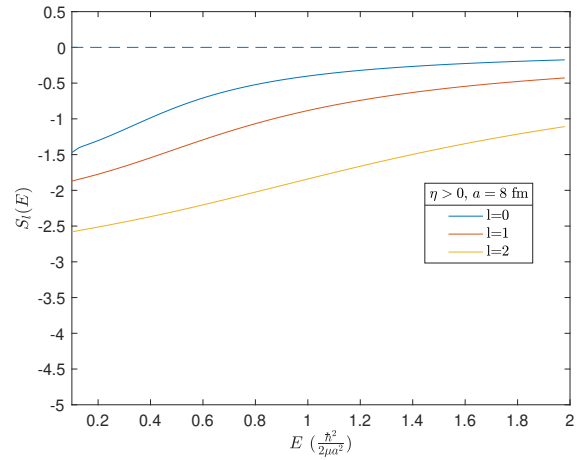which is always positive and an increasing function of E [21].
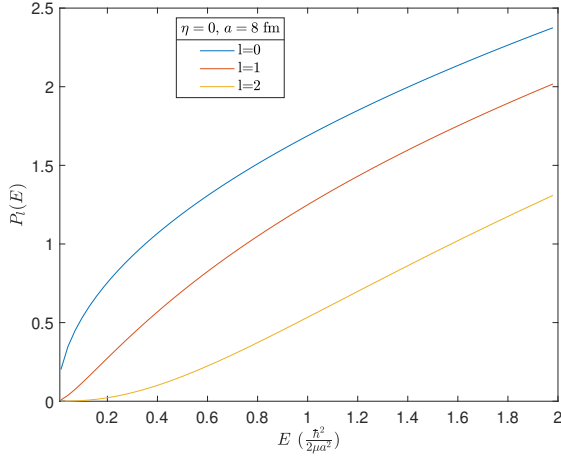
(a) $P_l(E)$ for $\eta = 0$ and $a = 8$ fm
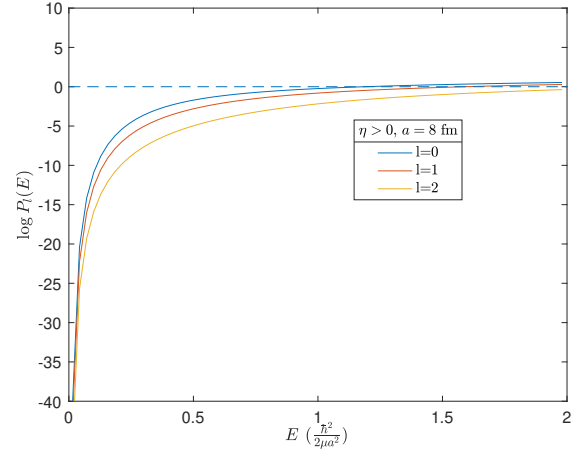
(b) $\log P_l(E)$ for $\eta > 0$ and $a = 8$ fm
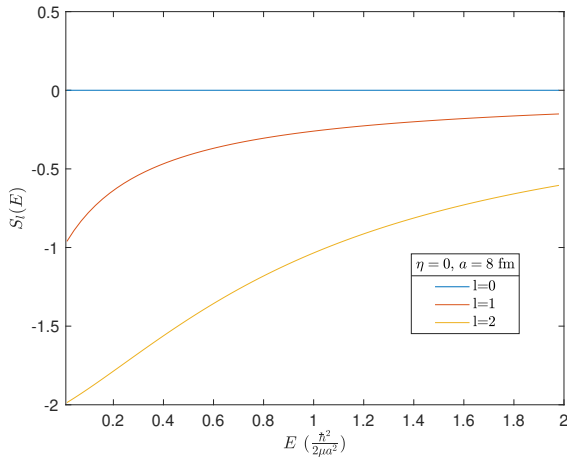
(c) $S_l(E)$ for $\eta = 0$ and $a = 8$ fm

(d) $S_l(E)$ for $\eta > 0$ and $a = 8$ fm

Figure 2.2: Graphical representation of the penetration factor $P_l(E)$ and shift factor $S_l(E)$, for angular momentum l and Sommerfeld parameter η.

The shift factor is:

$$S_l(E) = P_l(E)\Big[F_l(ka)F_l'(ka) + G_l(ka)G_l'(ka)\Big] \ , \tag{2.68}$$

and is always negative for $\eta \geq 0$. Although there is no available proof that it is always an increasing function of energy, no counterexample could be found by calculations in [1].

As it can be seen from figures 2.2a and 2.2b, penetration factors do not have a strong dependence on energy for the neutral case ($\eta = 0$), whereas they vary sharply (logarithmic scale is used) for low energy values in the repulsive case ($\eta > 0$), due to the Coulomb barrier that impedes penetration. The highest the angular momentum value l, the more intense the effect of the barrier, due to the centrifugal term.

From figures 2.2c and 2.2d, it is clear that shift factors have a smooth dependence on energy. Except for $l = 0$, this dependence is rather similar for both neutral and repulsive cases.

Using definition (2.66), the scattering matrix can be written as:

$$U_l(E) = e^{2i\delta_l} = e^{2i\phi_l} \frac{1 - (S_l - B)R_l + iP_lR_l}{1 - (S_l - B)R_l - iP_lR_l} \;, \tag{2.69}$$

or solving for the phase shift $\delta_l(E)$:

$$\delta_l(E) = \phi_l(E) + \arctan\left[\frac{P_lR_l}{1 - (S_l - B)R_l}\right] \;. \tag{2.70}$$

From this expressions, the internal wave function can be written:

$$u_l^{int}(r) = \frac{\hbar^2}{\mu a} e^{i(\delta_l - \frac{\pi}{2})} C_l \frac{\sqrt{kaP_l}}{|1 - (L_l - B)R_l|} \sum_{i,j=1}^{N} \varphi_i(a)\mathbf{C}_{ij}^{-1}\varphi_j(r) \;, \tag{2.71}$$

or for an orthonormal basis:

$$u_l^{int}(r) = \frac{\hbar^2}{\mu a} e^{i(\delta_l - \frac{\pi}{2})} C_l \frac{\sqrt{kaP_l}}{|1 - (L_l - B)R_l|} \sum_{n=1}^{N} \frac{\chi_{nl}(a)\chi_{nl}(r)}{E_{nl} - E} \;. \tag{2.72}$$

2.2.3 Resonances

In Nuclear Physics, a resonance is a peak of differential cross sections in scattering processes around a certain energy, called resonance energy. There is a great number of methods to study resonances. Regarding the R-matrix theory, one of these methods is letting B be complex, which leads to a simpler expression for the scattering matrix [22]. This approach allows direct calculation of resonance energies, which are its poles. However, this procedure requires iterations and the same results can also be interpreted with real values of the boundary parameter. This is why B will remain a real number, in particular $B = 0$ for simplicity in this case. One definition of the resonance energy E_R is those values for which $\delta_l - \phi_l = \frac{\pi}{2}$, so that conforming to relation (2.70) it is defined by the equation:

$$1 - S_l(E_R)R_l(E_R) = 0 \;, \tag{2.73}$$

which normally has to be solved by numerical methods. For the definition of the resonance width, one considers the collision matrix (2.69) at energies close to E_R. Carrying out a Taylor expansion of $S_l(E)R_l(E)$ provides the so-called Breit-Wigner approximation:

$$U_l^{BW}(E) \approx e^{2i\phi_l}\frac{E_R - E + i\Gamma(E)/2}{E_R - E - i\Gamma(E)/2} \ , \tag{2.74}$$

where the energy-dependent resonance width is:

$$\Gamma(E) = 2\frac{P_l(E)R_l(E)}{\frac{\mathrm{d}(S_lR_l)}{\mathrm{d}E}\big|_{E=E_R}} \ . \tag{2.75}$$

Since E_R does not coincide with the R-matrix poles, $R_l(E)$ is assumed to vary slowly enough for $E \approx E_R$ so that $R_l(E) \approx R_l(E_R)$. The width is then approximated by:

$$\Gamma(E) \approx 2\gamma^2 P_l(E) = \frac{P_l(E)}{P_l(E_R)}\Gamma(E_R) \ , \tag{2.76}$$

where γ^2 is the reduced width of the resonance and is given by:

$$\gamma^2 = \frac{R_l(E_R)}{\frac{\mathrm{d}(S_lR_l)}{\mathrm{d}E}\big|_{E=E_R}} \ . \tag{2.77}$$

It is now clear to see why it is called the reduced width, since it is the result of dividing the total width $\Gamma(E)$ by two times $P_l(E)$.

Equally, another way of studying resonances is considering an energy E close to a pole E_{nl} of the R-matrix. It is assumable that terms with $n' \neq n$ can be neglected in expression (2.58), so that the R-matrix is taken to be:

$$R_l(E) \approx \frac{\gamma_{nl}^2}{E_{nl} - E} \ , \tag{2.78}$$

and the phase shift is:

$$\delta_l \approx \phi_l + \arctan\left[\frac{\gamma_{nl}^2 P_l(E)}{E_{nl} - \gamma_{nl}^2 S_l(E_R) - E}\right] \ . \tag{2.79}$$

This expression can be directly compared to the Breit-Wigner form of the phase shift:

$$\delta_l^{BW} \approx \phi_l + \arctan\left[\frac{\Gamma(E)/2}{E_R - E}\right] \ , \tag{2.80}$$

which leads to definitions of the resonance energy:

$$E_R = E_{nl} - \gamma_{nl}^2 S_l(E_R) \ , \tag{2.81}$$

and of the formal width:

$$\Gamma(E) = 2\gamma_{nl}^2 P_l(E) \ , \tag{2.82}$$

where one finds it consistent to call $S_l(E)$ the shift factor as its appearance on equation (2.81) shifts E_{nl} to E_R. Let it be pointed out that since $P_l(E)$ varies slowly with energy, equation (2.76) makes it feasible to take $\Gamma(E) \approx \Gamma(E_R)$, so that when E takes values $E \mp \Gamma(E_R)/2$, the second term of the RHS of (2.80) will be equal to $\frac{\pi}{2} \mp \frac{\pi}{4}$ respectively. Therefore, the resonance width is approximated as the energy separation between the points for which $\delta_l - \phi_l$ is equal to $\frac{\pi}{4}$ and $\frac{3\pi}{4}$.

Using equations (2.60), (2.81) and (2.82), the internal wave function can be approximated near a resonance:

$$u_l^{int}(r) \approx e^{i(\delta_l - \frac{\pi}{2})} C_l \left[\frac{\hbar v \Gamma(E)}{(E_R - E)^2 + (\frac{\Gamma(E)}{2})^2} \right]^{1/2} \chi_{nl}(r) \; , \tag{2.83}$$

which is proportional to an eigenfunction (2.60) of operator $H_l + \mathcal{L}_{B=0}(r)$ (see subsection 2.2.1), whose proportionality constant presents the usual Lorentzian energy dependence of a resonance.

2.2.4 Basis functions

The set of basis functions $\{\varphi_j(r)\}_{j=1}^{N}$ over which function (2.19) can be expanded is chosen in various ways. In this survey only two set of functions are used: sine functions and Lagrange functions [1]. Both of these sets share the property that their elements are all zero at $r = 0$.

(i) Sine functions. They are defined by:

$$\varphi_j(r) = \sqrt{\frac{2}{a}} \sin \left[\frac{\pi r}{a} (j - \frac{1}{2}) \right] \; ; \; j = 1, \ldots, N \; , \tag{2.84}$$

whose overlaps are:

$$\langle \varphi_i | \varphi_j \rangle = \int_0^a \mathrm{d}r \varphi_i(r) \varphi_j(r) = \delta_{ij} \; ; \; i, j = 1, \ldots, N \; , \tag{2.85}$$

and whose kinetic-energy matrix elements for $l = 0$ read:

$$\langle \varphi_i | T_0 | \varphi_j \rangle = \int_0^a \mathrm{d}r \varphi_i(r) T_0 \varphi_j(r) = \frac{\hbar^2}{2\mu a^2} \frac{\pi^2}{2} \left(i - \frac{1}{2} \right)^2 \delta_{ij} \; ; \; i, j = 1, \ldots, N \; . \tag{2.86}$$

Matrix elements of $\mathcal{L}_{B=0}(r)$ are zero and Coulomb potential matrix elements are analytical for these functions. When $l > 0$ calculations are required, the centrifugal potential term appearing in kinetic energy (2.7):

$$V_{\text{cent},l}(r) = \frac{\hbar^2}{2\mu} \frac{l(l+1)}{r^2} \; ; \; T_l = T_0 + V_{\text{cent},l} \; , \tag{2.87}$$

is added to the total potential V. These basis functions simulate the oscillating behaviour of the internal wave function near $r = a$, nevertheless their derivative is always zero at this point,

$$\varphi'_j(a) = 0 \; ; \; j = 1, \ldots, N \; , \tag{2.88}$$

which turns out to be an inconvenience when matching the internal and external wave functions. Wave function derivability at $r = a$ is not ensured and hence the phase shifts are expected to have poor accuracy.

(ii) Lagrange functions. These functions are defined in the $(0, a)$ interval as:

$$\varphi_j(r) = (-1)^{N+j}(\frac{r}{ax_j})^n \frac{\sqrt{ax_j(1 - x_j)}}{r - ax_j} P_N(\frac{2r}{a} - 1) \; ; \; j = 1, \ldots, N \; , \tag{2.89}$$

where P_N is the Legendre polynomial of order N, and the numbers x_j are the N zeros satisfying:

$$P_N(2x_j - 1) = 0 \; . \tag{2.90}$$

The $(r/ax_j)^n$ factor is useful for avoiding singularities at $r = 0$, and $n = 1$ is taken for two-body calculations, which ensures $u_l^{int}(0) = 0$. Using the Gauss quadrature approximation of order N, a great advantage of this choice is that one obtains simple matrix elements which produce accurate results. Namely, using this approximation overlaps read [1]:

$$\langle \varphi_i | \varphi_j \rangle = \int_0^a \mathrm{d}r \varphi_i(r)\varphi_j(r) \approx \delta_{ij} \; ; \; i, j = 1, \ldots, N \; , \tag{2.91}$$

and potential matrix elements take the form:

$$\langle \varphi_i | V | \varphi_j \rangle = \int_0^a \mathrm{d}r \varphi_i(r)V(r)\varphi_j(r) \approx V(ax_i)\delta_{ij} \; ; \; i, j = 1, \ldots, N \; , \tag{2.92}$$

where V may include the centrifugal term. For this basis, matrix elements of operator $T_0 + \mathcal{L}_{B=0}(r)$ are calculated as [1]:

(a) For $i = j$

$$\langle \varphi_i | T_0 + \mathcal{L}_{B=0} | \varphi_j \rangle = \frac{(4N^2 + 4N + 3)x_i(1 - x_i) - 6x_i + 1}{3a^2 x_i^2 (1 - x_i)^2} \; . \tag{2.93}$$

(b) For $i \neq j$

$$\langle \varphi_i | T_0 + \mathcal{L}_{B=0} | \varphi_j \rangle = \frac{(-1)^{i+j}}{a^2 \left[x_i x_j (1 - x_i)(1 - x_j) \right]^{1/2}} \tag{2.94}$$

$$\times \left[N^2 + N + 1 + \frac{x_i + x_j - 2 x_i x_j}{(x_i - x_j)^2} - \frac{1}{1 - x_i} - \frac{1}{1 - x_j} \right] . \tag{2.95}$$

Chapter 3

Applications of the R-matrix theory

In this chapter the calculable R-matrix method is applied to scattering by a potential. In particular, two resonances are studied employing the previous choices of basis functions: the ^{12}C+p system $1/2^+$, and ^{10}Be+n system $5/2^+$ resonances.

In both of the previous cases, two-body collisions regardless of internal structure are assumed, and the potential through which these particles interact is $V(r)$, which can be l-dependent (spin-orbit interaction and centrifugal term). The Numerov method provides a computational technique to solve the Schrödinger equation exactly [23–25], likewise the Schrödinger equation for the system ^{10}Be+n is numerically solved in [6]. Results obtained following numerical methods in these papers will be called 'exact' from now on in this work, and they are compared to the R-matrix method results regarding the ^{12}C+p system in section 3.1. Once convergence is obtained, the same program is applied to the ^{10}Be+n system, and R-matrix and exact results are compared again in section 3.2.

All computational algorithms and calculations have been designed and carried out by means of the software MATLAB®.

In order to find phase shifts (2.70), several intermediate calculations need to be made step-by-step. The followed procedure can be described by these instructions:

(i) First of all, orthonormality of basis functions must be checked. Accordingly, relations (2.85) and (2.91) were verified.

(ii) Secondly, with $a = 8$ fm, $N = 7$, and $E = 1$ MeV for instance, matrix elements (2.92) and those of operator $T_0 + \mathcal{L}_{B=0}(r)$ are computed.

(iii) Once matrix elements are obtained, $\mathbf{C}$ matrix (2.45) can be calculated as well as its

inverse.

(iv) Following relation (2.51), the R-matrix $R_l(E)$ is obtained.

(v) Knowing $R_l(E)$ allows direct calculation of phase shifts according to equation (2.70), and from there on these quantities are known for the particular E value initially chosen.

(vi) Schematic repetition of this procedure for each E in $(0,2)$ MeV will yield δ_l as a function of E.

(vii) Once $\delta_l(E)$ is obtained, one tests different a values, and for each one of them N is increased until convergence is reached. The a value for which this last condition occurs offers precise results (in comparison with exact values) and is the chosen a value.

When phase shifts are determined as a function of E, other relevant quantities involved in the scattering process can be deduced. The resonance energy is obtained by means of equation (2.73), and resonance widths are estimated at the Breit-Wigner approximation, where the energy-dependent width (2.75) is evaluated at $E = E_R$ to obtain the resonance width. In addition, partial wave functions are directly determined with relation (2.71).

3.1 ^{12}C+p system: $1/2^+$ Continuum

The system ^{12}C+p ($J^\pi = \frac{1}{2}^+$, $l = 0$) possesses a narrow resonance, $\Gamma = 37$ keV, at $E_R = 0.42$ MeV [1, 26]. Studying a resonance is going to allow the verification of the R-matrix method's accuracy, since setting $\delta_{l=0} - \phi_{l=0} = \pi/2$ should send back the E_R value as seen in equation (2.73). For this system, calculations will be performed using the following values:

$$\frac{\hbar^2}{2\mu} = 22.464 \text{ MeV fm}^2 \; ; \; e^2 = 1.44 \text{ MeV fm} , \qquad (3.1)$$

and potentials will be chosen from equation (4.14) in [1]:

$$V_N(r) = -V_{N,0} \exp\left[-\left(\frac{r}{b}\right)^2\right] \text{ (Nuclear potential) },$$ (3.2)

$$V_{N,0} = 73.8 \text{ MeV} ; \ b = 2.70 \text{ fm} ,$$

$$V_C(r) = \frac{Z_1 Z_2 e^2}{r} = 6\frac{e^2}{r} \text{ (Coulomb potential) },$$ (3.3)

$$V(r) = V_N(r) + V_C(r) \text{ (Total potential) }.$$ (3.4)

In figure 3.1 all potentials describing this resonance are graphically represented.
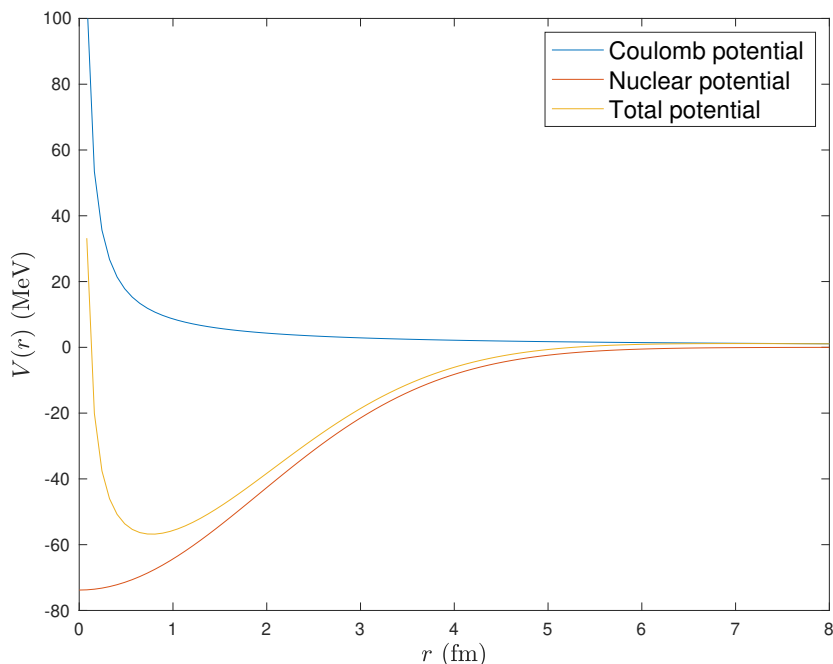
Figure 3.1: Potentials used for the ^{12}C+p system.

In figure 3.2 exact and R-matrix results for the phase shift $\delta_0(E)$ are displayed. Lagrange results for $N = 15$ in figure 3.2b overlap those for $N = 10$. R-matrix calculations have been performed with both choices of basis functions discussed in subsection (2.2.4) so that greater accuracy of Lagrange functions over that of sine functions may be pointed out. As in [1], the channel radius is chosen as $a = 8$ fm in figures 3.2a and 3.2b, beyond which it is reasonable to consider negligible nuclear interactions. In figure 3.2a sine functions are used. Curves of the phase shift depending on N are represented and one may notice that they provide a satisfactory result even for low values of N.

In the case of Lagrange functions, figure 3.2b shows how convergence is reached as a function of N. It turned out that $N = 10$ is the minimum value that produces precise

results.

Convergence as a function of a is shown for sine functions in figure 3.2c, and for Lagrange functions in 3.2d.

Table 3.1 displays explicit $\delta_0(E)$ values obtained with various parameter settings. It is possible to contrast Lagrange with sine results, confirming predictions that Lagrange functions would bear better outcomes. Namely, one may verify that even phase shifts values for $N = 20$ with sine functions are less precise than those for $N = 15$ with Lagrange functions.
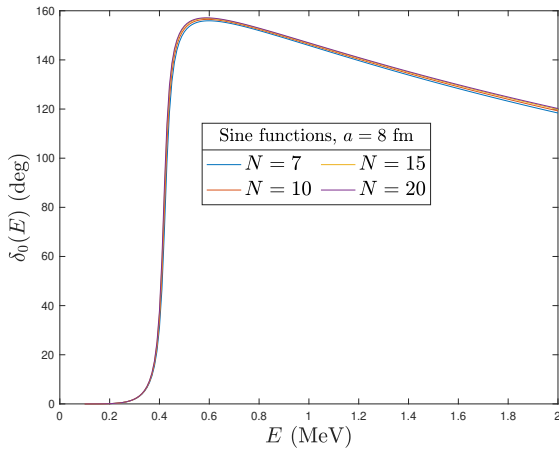
(a) Convergence with sine functions depending on N, $a = 8$ fm.
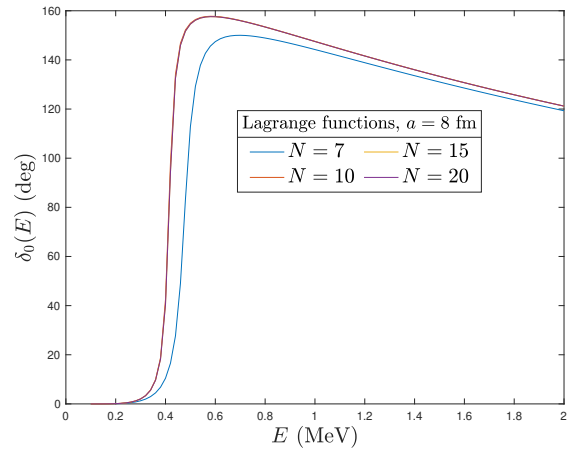
(b) Convergence with Lagrange functions depending on N, $a = 8$ fm.
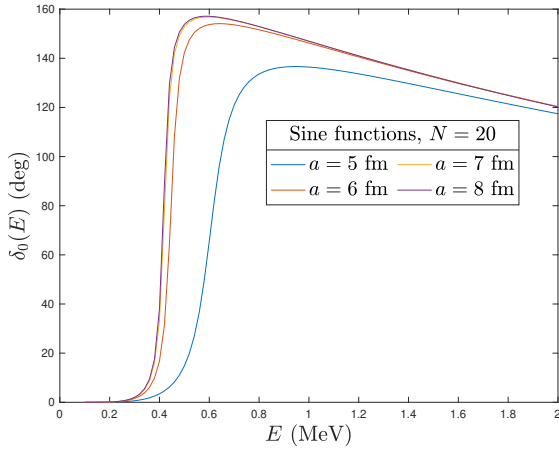
(c) Convergence with sine functions depending on a, $N = 20$.
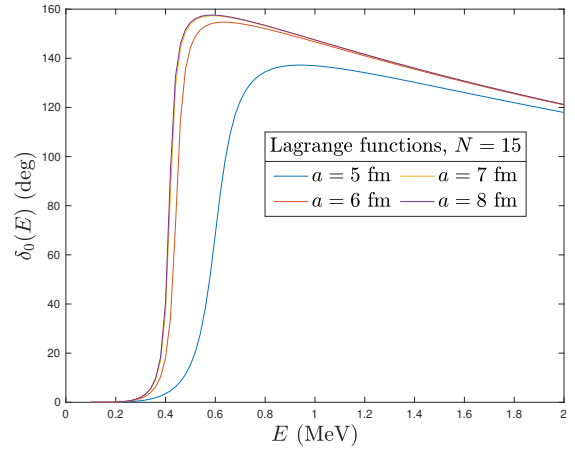
(d) Convergence with Lagrange functions depending on a, $N = 15$.

Figure 3.2: Graphical representation of $\delta_0(E)$: R-matrix results with several N and a choices for both sine and Lagrange functions.

E (MeV)	Phase shift $\delta_0(E)(°)$				
	Exact	$N=7$	$N=10$	$N=15$	$N=20$
	Lagrange functions				
0.5	154.66	112.90	154.94	154.59	
1.0	147.48	144.22	147.55	147.48	
1.5	133.30	311.02	133.35	133.30	
2.0	121.18	299.30	121.23	121.18	
	Sine functions				
0.5	154.66	151.42	152.59	153.39	153.82
1.0	147.48	145.88	146.39	146.74	146.95
1.5	133.30	131.05	131.74	132.23	132.53
2.0	121.18	118.39	119.24	119.86	120.22

Table 3.1: Phase shifts $\delta_0(E)$ for the ^{12}C+p system, ($a = 8$ fm) for Lagrange and sine basis. Exact results are found in [1, 26].

Resonance energy E_R (MeV)				Width of the resonance $\Gamma(E_R)$ (keV)			
$N=7$	$N=10$	$N=15$	$N=20$	$N=7$	$N=10$	$N=15$	$N=20$
Lagrange functions				Lagrange functions			
0.482	0.418	0.418		65.4	37.8	37.7	
Sine functions				Sine functions			
0.425	0.423	0.420	0.420	41.5	40.3	39.1	39.0

Table 3.2: Resonance energy values E_R and resonance widths $\Gamma(E_R)$ for the ^{12}C+p ($l = 0$) system, ($a = 8$ fm) for Lagrange and sine basis, ($E_R^{exp} = 0.42$ MeV, $\Gamma^{exp} = 37$ keV [1]).

Table 3.2 shows values of E_R and $\Gamma(E_R)$ obtained with several parameter choices. In this case, $N = 7$ values do not reproduce exact data for Lagrange functions very precisely, whereas in all other cases both basis functions offer satisfactory results.

Figure 3.3 contains graphical representations of the partial wave function $u_0(r)$ for both basis functions choices depending on the N value, with $a = 8$ fm and for two particular energies: $E = 1$ MeV and $E = E_R$. Comparing left and right figures, it is plainly seen how Lagrange functions ensure wave function derivability and sine functions are not capable of that. This fact should entail a great setback in phase shift precision for sine functions, nevertheless, from figures 3.2a, 3.2c and table 3.1 it is shown that even these functions provided accurate results.
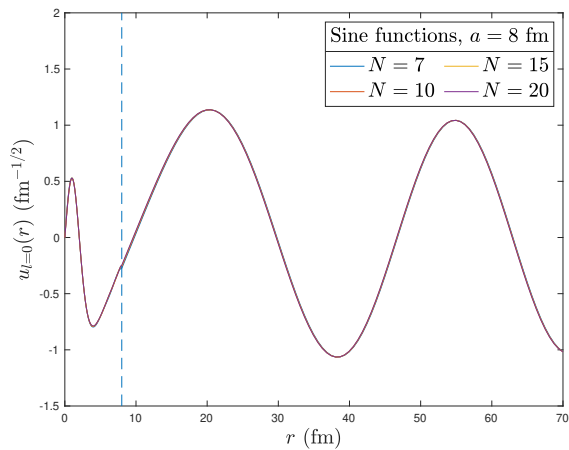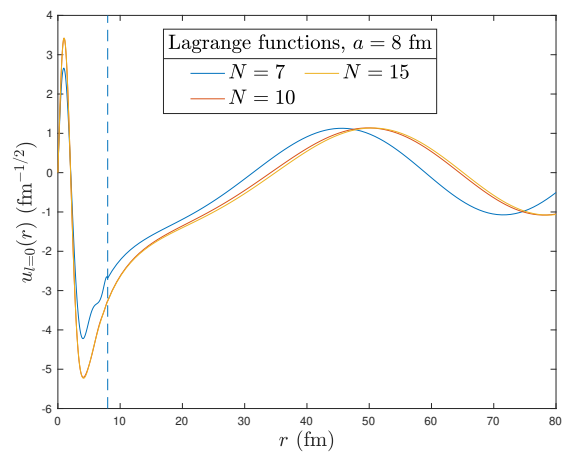
(a) $u_{l=0}$ for $E = 1$ MeV with sine functions.
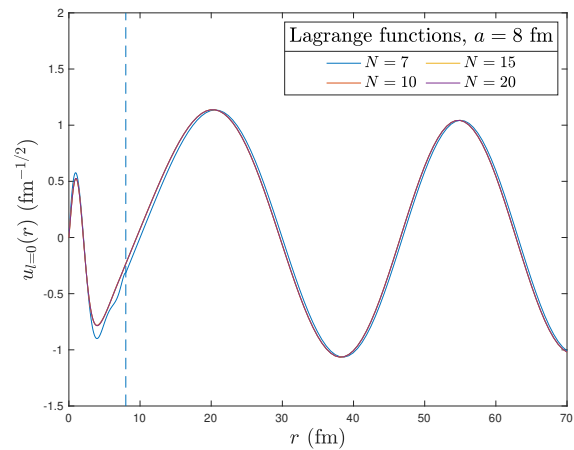
(b) $u_{l=0}$ for $E = 1$ MeV with Lagrange functions.
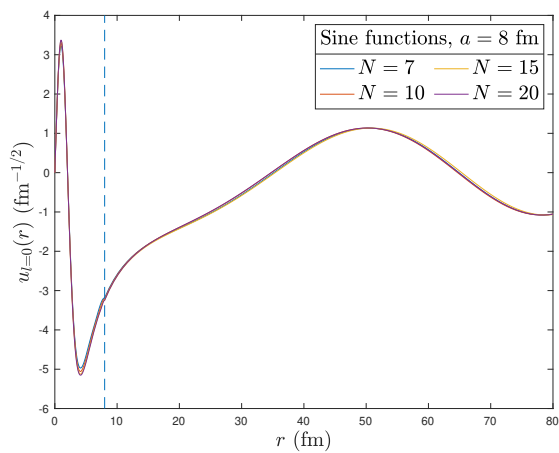
(c) $u_{l=0}$ at resonance energy $E = E_R$ MeV with sine functions.

(d) $u_{l=0}$ at resonance energy $E = E_R$ MeV with Lagrange functions.

Figure 3.3: ^{12}C+p, ($l = 0$) wave functions at $a = 8$ fm, depending on N for $E = 1$ MeV and respective $E = E_R$ values.

3.2 $\quad{}^{10}$Be+n system: $5/2^+$ Continuum

The system ^{10}Be+n ($J^\pi = \frac{5}{2}^+$, $l = 2$) also possesses a narrow resonance, $\Gamma = 100 \pm 20$ keV, at $E_R = 1.274 \pm 0.018$ MeV [27, 28]. For this system, calculations will be performed using:

$$\frac{\hbar^2}{2\mu} = 22.809 \text{ MeV fm}^2 \ , \tag{3.5}$$

and the potentials are taken from equations (5), (14) and (16) in [6]:

$$V_0(r) = -V_{l=2} f_{R_0,b}(r) \text{ (Nuclear potential)} \tag{3.6}$$

$$f_{R_0,b}(r) = \left[1 + \exp\left(\frac{r - R_0}{b}\right)\right]^{-1} ; V_{l=2} = 62.52 \text{ MeV} ; R_0 = 2.585 \text{ fm} ; b = 0.6 \text{ fm} \ ,$$

$$V_{S-O}(r) = \vec{L} \cdot \vec{S} \frac{V_{LS}}{r} \frac{\mathrm{d} f_{R_0,b}(r)}{\mathrm{d}r} \text{ (Spin-orbit coupling)} \ , \tag{3.7}$$

$$\vec{L} \cdot \vec{S} = \frac{1}{2}\left[\vec{J}^2 - \vec{L}^2 - \vec{S}^2\right] ; V_{LS} = 21.0 \text{ MeV fm}^2 \ ,$$

$$V_{cent}(r) = \frac{\hbar^2}{2\mu} \frac{l(l+1)}{r^2} \text{ (Centrifugal potential)} \ , \tag{3.8}$$

$$V(r) = V_0(r) + V_{S-O}(r) + V_{cent}(r) \ , \tag{3.9}$$

where $\vec{L}$, $\vec{S}$, and $\vec{J} = \vec{L} + \vec{S}$ are the relative orbital angular momentum of the system, the neutron spin and the total angular momentum of the system respectively. $\vec{L} \cdot \vec{S} = 1$ since $J = \frac{5}{2}$ is being considered.

Just like in the previous case, in figure 3.4 all potentials describing this resonance are plotted, as well as their sum. In figure 3.5 R-matrix results for $\delta_2(E)$ are displayed. As in the precedent case, R-matrix calculations have been performed with both choices of basis functions. The channel radius has a larger value this time in figures 3.5a and 3.5b. It turned out $a = 10$ fm provided convergence.

In figure 3.5a sine functions are used. Graphical representations of the phase shift depending on N are given and convergence is visibly reached at $N = 10$.

As to Lagrange functions, figure 3.5b features convergence as a function of N. In this case, $N = 15$ is the minimum value that produces accurate results, since an increase in a entails an increase in N for precise results.

Again, convergence as a function of a is shown for sine functions in figure 3.5c, and for Lagrange functions in 3.5d. All data converge so rapidly for such a high value of N, that curves are superimposed.
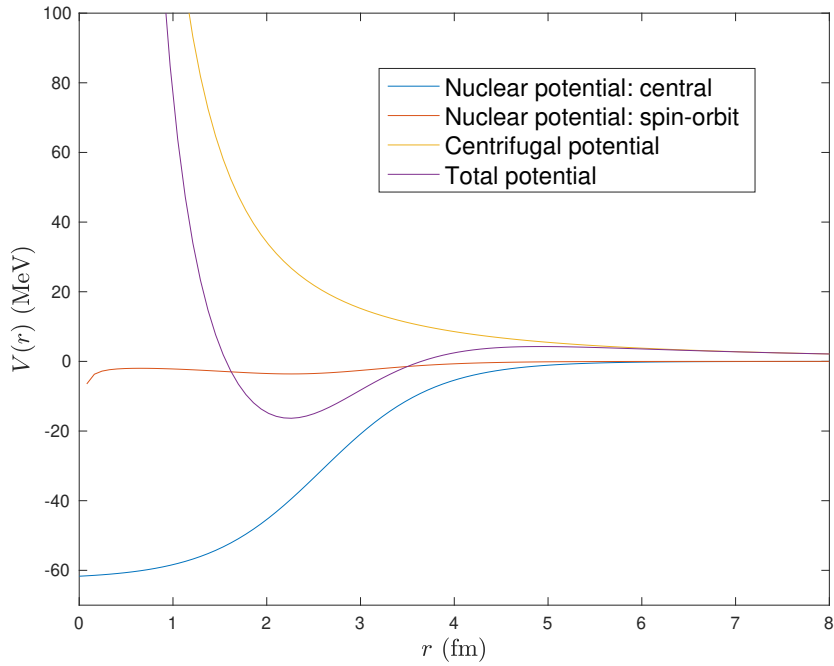
Figure 3.4: Potentials used for the ^{10}Be+n system.

Table 3.3 shows certain $\delta_2(E)$ values obtained with various parameter settings. No exact results for this quantity are shown in this table to serve as comparison data, however, as it has been shown, results with higher precision are expected using Lagrange functions. In this case, accuracy will be tested solely on the values of E_R. Table 3.4 shows values of E_R and $\Gamma(E_R)$ obtained with different parametric values. As one may corroborate, increasing N values reproduce experimental data for Lagrange functions more precisely.

Figure 3.6 contains graphical representations of the partial wave function $u_2(r)$ for both basis functions, different N values, with $a = 10$ fm and for two particular energies: $E = 1$ MeV and $E = E_R$. Once more, visualising left and right figures, it is directly seen how Lagrange functions establish wave function derivability, which sine functions are not able to. One may also confirm that $N = 7$ is too low a N value for such a great a.
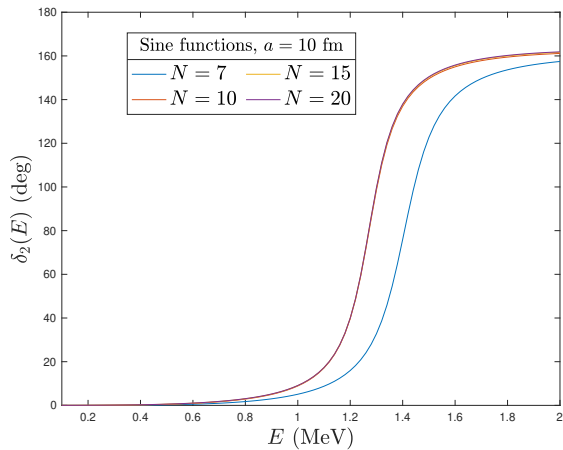
(a) Convergence with sine functions depending on N, $a = 10$ fm.
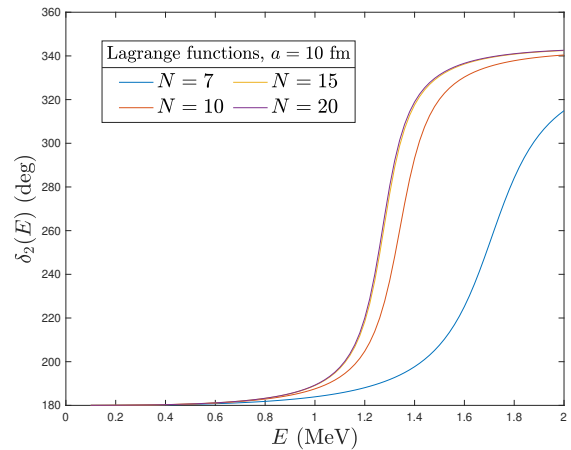
(b) Convergence with Lagrange functions depending on N, $a = 10$ fm.
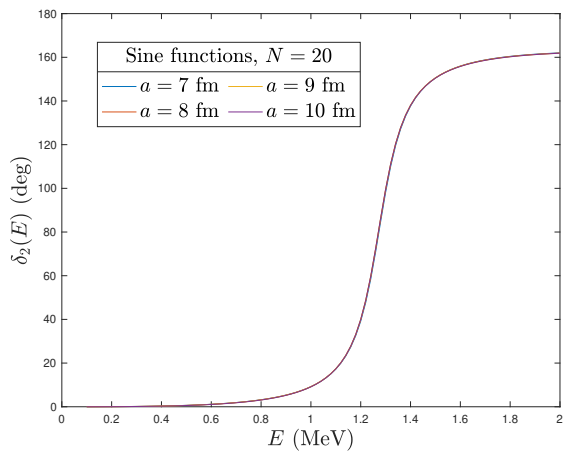
(c) Convergence with sine functions depending on a, $N = 20$.
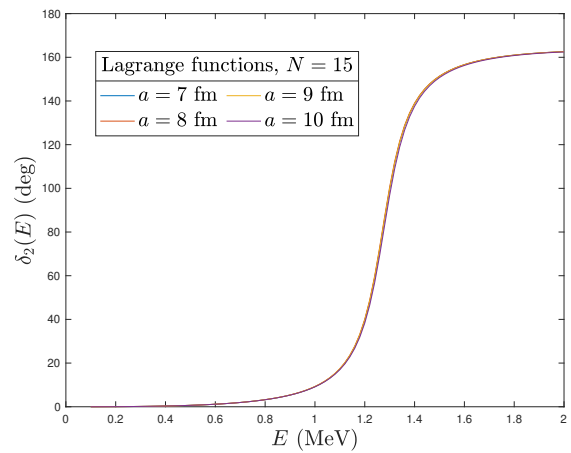
(d) Convergence with Lagrange functions depending on a, $N = 15$.

Figure 3.5: Graphical representation of $\delta_2(E)$: R-matrix results with several N and a choices for both sine and Lagrange functions.

E (MeV)	Phase shift $\delta_0(E)(°)$			
	$N = 7$	$N = 10$	$N = 15$	$N = 20$
Lagrange functions				
0.5	0.45	0.61	0.65	0.66
1.0	3.91	7.57	9.11	9.28
1.5	27.61	140.15	150.71	151.33
2.0	134.92	160.43	162.46	162.59
Sine functions				
0.5	0.24	0.48	0.54	0.58
1.0	5.10	8.89	9.05	9.11
1.5	122.70	149.58	150.18	150.46
2.0	157.46	161.14	161.63	161.89

Table 3.3: Phase shifts $\delta_2(E)$ for the ^{10}Be+n system, ($a = 10$ fm) for Lagrange and sine basis.

Resonance energy E_R (MeV)				Width of the resonance $\Gamma(E_R)$ (keV)			
$N = 7$	$N = 10$	$N = 15$	$N = 20$	$N = 7$	$N = 10$	$N = 15$	$N = 20$
Lagrange functions				Lagrange functions			
1.635	1.312	1.254	1.251	379	195	172	169
Sine functions				Sine functions			
1.375	1.250	1.250	1.250	210	172	173	173

Table 3.4: Resonance energy values E_R and resonance widths $\Gamma(E_R)$ for the ^{10}Be+n ($l = 2$) system, ($a = 10$ fm) for Lagrange and sine basis ($E_R^{\text{exact}} = 1.274$ MeV, $\Gamma^{\text{exact}} \sim 162$ keV [6]).
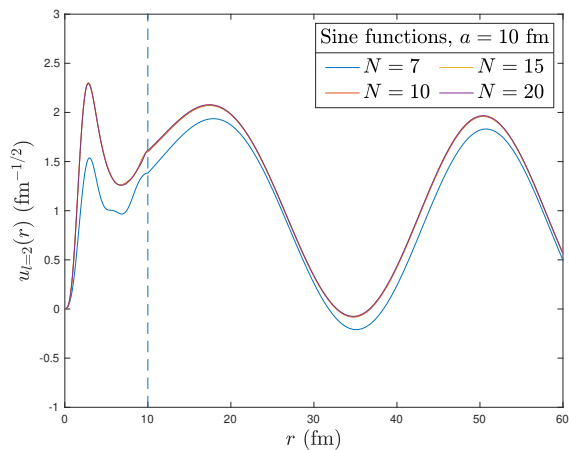
(a) $u_{l=2}$ for $E = 1$ MeV with sine functions.
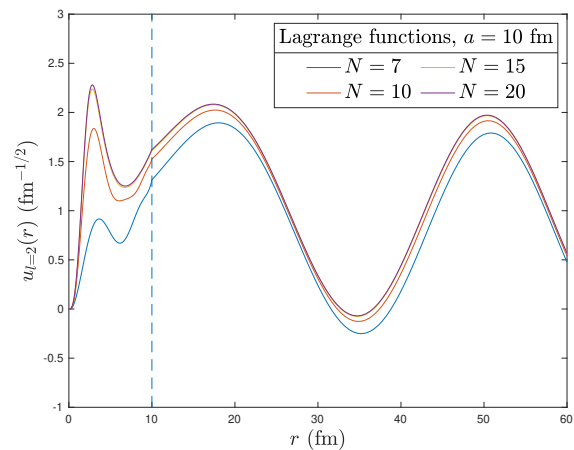
(b) $u_{l=2}$ for $E = 1$ MeV with Lagrange functions.
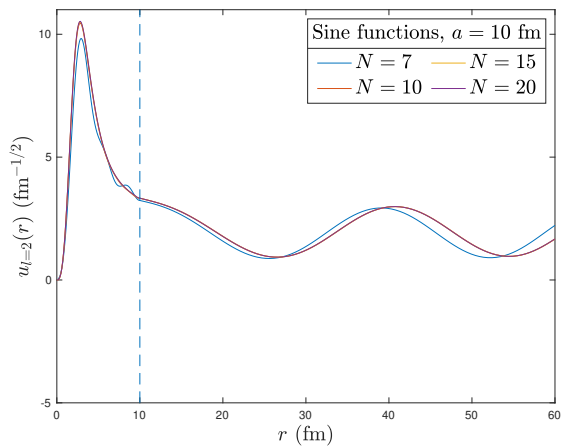
(c) $u_{l=2}$ at resonance energy $E = E_R$ MeV with sine functions.
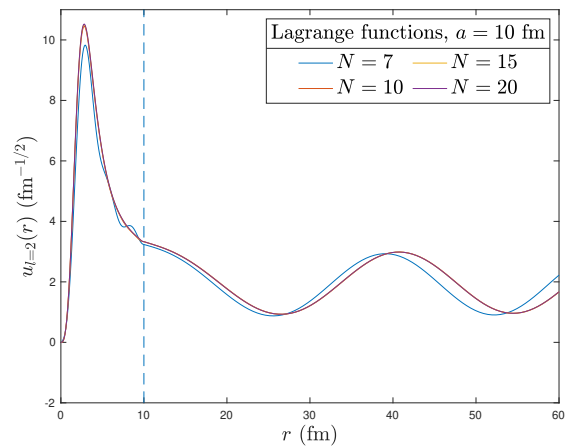
(d) $u_{l=2}$ at resonance energy $E = E_R$ MeV with Lagrange functions.

Figure 3.6: ^{10}Be+n, $(l = 2)$ wave functions at $a = 10$ fm, depending on N for $E = 1$ MeV and respective $E = E_R$ values.

Chapter 4

Conclusions

In this work, the R-matrix method has been studied and it has been employed in the resolution of two simple quantum-mechanical problems: the description of two resonant states of two-body systems. After an outline of the fundamental concepts of scattering theory, an extensive presentation of the theory has been shown, highlighting important quantities such as the R-matrix $R_l(E)$ itself, the Bloch operator and the phase shift. By the same token, important definitions such as that of a resonance, and its corresponding energy and resonance width have been pointed out.

Applications to the two particular cases of the ^{12}C+p and ^{10}Be+n resonances have followed, results have been displayed explicitly, and compared to values which can either be found by numerical methods or have been observed experimentally.

In relation to the ^{12}C+p system, a resonance has been studied for the case in which $l = 0$. Regarding sine functions, it has been seen that phase shifts are obtained with satisfactory convergence for $N = 20$ and $a = 8$ fm. For Lagrange functions convergence was obtained for $N = 15$ and $a = 8$ fm. Moreover, it has been verified that the partial wave functions is not derivable when the sine function basis is employed, whereas for Lagrange functions derivability at $r = a$ is ensured using $N \geq 10$ and $a = 8$ fm.

With respect to the ^{10}Be+n resonance, $l = 2$ in that case, so a centrifugal term is added to the total potential. Although phase shifts are not compared to exact results, in section 3.2 comparisons of exact data of E_R and $\Gamma(E_R)$ with R-matrix results are made, using different N and a values. As it has been confirmed, $N = 20$ and $a = 10$ fm produce best results for both basis choices. As to wave functions, the same values hold for converged curves. Again, it is seen that sine functions do not provide the wave function

with derivability at $r = a$, whilst Lagrange functions are suitable for that feature.

As seen in the introduction, the R-matrix theory has two variants: the phenomenological and the calculable R-matrix. Whereas the phenomenological version was uniquely introduced to fit experimental data in nuclear processes, the calculable version, which has substantiated the core of this work, has been extended over the years from Atomic to Nuclear Physics problems due to its straightforward procedure to solve the Schrödinger equation.

Frequent criticisms regarding the R-matrix theory have often been related to the interpretation of the channel radius a, and the apparent poor convergence of results.

As it has been shown in chapter 3, the first of these two detrimental judgements has been revoked, since physical results become independent of the channel radius for sufficiently large values of it.

On the other hand, it has been proved that convergence is at all times achieved for an adequate size of the internal function basis N. The misconception that R-matrix calculations do not provide converging results lies on requiring these functions to satisfy specific boundary conditions. Whilst it is acceptable to proceed this way when the bases are infinite, it leads to inconsistencies when the number of functions is truncated (see discussion in section 3.5 of [1]). The introduction of the Bloch operator allows usage of finite bases with wide-ranging behaviours at the boundary in order to prevent this problem.

Thus, it has been verified that R-matrix calculations provide satisfactory results reducing the number of relevant parameters, which makes this theory a major asset among quantum-mechanical tools to describe collisions.

Furthermore, although it has not been reviewed in this dissertation, the calculable R-matrix version can likewise be applied to bound state problems.

Bibliography

[1] P. Descouvemont and D. Baye. The R-matrix theory. *Reports on progress in physics*, 73(3):036301, 2010.

[2] E.P. Wigner. Resonance reactions and anomalous scattering. *Physical Review*, 70 (1-2):15, 1946.

[3] E.P. Wigner. Resonance reactions. *Physical Review*, 70(9-10):606, 1946.

[4] E.P. Wigner and L. Eisenbud. Higher angular momenta and long range interaction in resonance reactions. *Physical Review*, 72(1):29, 1947.

[5] P.L. Kapur and R. Peierls. The dispersion formula for nuclear reactions. *Proceedings of the Royal Society of London. Series A. Mathematical and Physical Sciences*, 166 (925):277, 1938.

[6] P. Capel, G. Goldstein, and D. Baye. Time-dependent analysis of the breakup of ^{11}Be on ^{12}C at 67 MeV/nucleon. *Physical Review C*, 70(6):064605–3, 2004.

[7] D. Baye. An introduction to the R-matrix method. `http://nucleartheory.eps.surrey.ac.uk/Talent_6_Course/Other_materials/lectures/Trento_Baye_Rmatrix.pdf`, last visited on 15/06/2021.

[8] M.E. Haglund and D. Robson. Intermediate structure and channel coupling theory. *Physics Letters*, 14(3):225, 1965.

[9] P.J.A. Buttle. Solution of coupled equations by R-matrix techniques. *Physical Review*, 160(4):719, 1967.

[10] P.G. Burke and W.D. Robb. The R-matrix theory of atomic processes. In *Advances in atomic and molecular physics*, volume 11, page 143. Elsevier, 1976.

[11] P.G. Burke and K.A. Berrington. Atomic and molecular processes: an R-matrix approach. 1993.

[12] J. Tennyson. Electron–molecule collision calculations using the R-matrix method. *Physics Reports*, 491(2-3):29, 2010.

[13] G. Goertzel. Resonance reactions involving Dirac-type incident particles. *Physical Review*, 73(12):1463, 1948.

[14] I.P. Grant. The Dirac operator on a finite domain and the R-matrix method. *Journal of Physics B: Atomic, Molecular and Optical Physics*, 41(5):055002, 2008.

[15] C. Cohen-Tannoudji, B. Diu, and F. Laloë. *Mécanique Quantique-Tome 2*. EDP Sciences, 2021.

[16] A. Messiah. *Mécanique Quantique. 1*. Hermann, 1962.

[17] F.J.Y. Muñoz. *Mecánica Cuántica: teoría general*. Grupo Planeta (GBS), 2003.

[18] M. Abramowitz and I.A. Stegun. *Handbook of mathematical functions with formulas, graphs, and mathematical tables*, volume 55. US Government printing office, 1964.

[19] DLMF. *NIST Digital Library of Mathematical Functions*. http://dlmf.nist.gov/, Release 1.1.1 of 2021-03-15. URL `http://dlmf.nist.gov/`. last visited on 15/06/2021.

[20] C. Bloch. Une formulation unifiée de la théorie des réactions nucléaires. *Nuclear Physics*, 4:503, 1957.

[21] A.M. Lane and R.G. Thomas. R-matrix theory of nuclear reactions. *Reviews of Modern Physics*, 30(2):257, 1958.

[22] P.L. Kapur and R. Peierls. The dispersion formula for nuclear reactions. *Proceedings of the Royal Society of London. Series A. Mathematical and Physical Sciences*, 166 (925):277, 1938.

[23] N. Michel. A simple and efficient numerical scheme to integrate non-local potentials. *The European Physical Journal A*, 42(3):523, 2009.

[24] J.M. Hutson. Coupled channel methods for solving the bound-state Schrödinger equation. *Computer Physics Communications*, 84(1-3):1, 1994.

[25] J. Raynal. Computing as a language of physics. *IAEA, Vienna*, 281, 1972.

[26] F. Ajzenberg-Selove. Energy levels of light nuclei A= 13-15. *Nuclear Physics A*, 523 (1):1, 1991.

[27] F. Ajzenberg-Selove. Energy levels of light nuclei A= 5-10. *Nuclear Physics A*, 490 (1):1, 1988.

[28] G. Audi and A.H. Wapstra. The 1995 update to the atomic mass evaluation. *Nuclear Physics A*, 595(4):409, 1995.

List of Figures

List of Tables